Chemical Abundances of the Highly Obscured Galactic Globular Clusters 2MASS GC02 and Mercer 5

Francisco Peñaloza

Insituto de Fisica y Astronomia, Facultad de Ciencias, Universidad de Valparaiso

Av. Gran Bretana 1111, Valparaiso, Chile

francisco.penaloza@uv.cl

Peter Pessev[1]

Instituto de Astrofísica de Canarias (IAC); Gran Telescopio Canarias (GRANTECAN)

E-38205 La Laguna, Tenerife, Spain

peter.pessev@gtc.iac.es

Sergio Vaśquez

Instituto de Astrofísica, Pontifica Universidad Católica de Chile; Milenium Institute of Astrophysics, MAS

Av. Vicuña Mackenna 4860, Santiago, Chile

svasquez@astro.puc.cl

Jura Borissova, Radostin Kurtev

Insituto de Fisica y Astronomia, Facultad de Ciencias, Universidad de Valparaiso; Milenium Institute of Astrophysics, MAS

Av. Gran Bretana 1111, Valparaiso, Chile

jura.borissova@uv.cl, radostin.kurtev@uv.cl

and

Manuela Zoccali

Instituto de Astrofísica, Pontifica Universidad Católica de Chile; Milenium Institute of Astrophysics, MAS

Av. Vicuña Mackenna 4860, Santiago, Chile

mzoccali@astro.puc.cl

Received ______________; accepted ______________

Submitted to PASP

ABSTRACT

We present the first high spectral resolution abundance analysis of two newly discovered Galactic globular clusters, namely Mercer 5 and 2MASS GC02 residing in regions of high interstellar reddening in the direction of the Galactic center. The data were acquired with the Phoenix high-resolution near-infrared echelle spectrograph at Gemini South (R $\sim$ 50000) in the 15500.0 - 15575.0 spectral region. Iron, Oxygen, Silicon, Titanium and Nickel abundances were derived for two red giant stars, in each cluster, by comparing the entire observed spectrum with a grid of synthetic spectra generated with MOOG. We found [Fe/H] values of -0.86 ± 0.12 and -1.08 ± 0.13 for Mercer 5 and 2MASS GC02 respectively. The [O/Fe], [Si/Fe] and [Ti/Fe] ratios of the measured stars of Mercer 5 follow the general trend of both bulge field and cluster stars at this metallicity, and are enhanced by $\geq +\ 0.3$. The 2MASS GC02 stars have relatively lower ratios, but still compatible with other bulge clusters. Based on metallicity and abundance patterns of both objects we conclude that these are typical bulge globular clusters.

Subject headings: globular clusters: individual (2MASS GC02, Mercer 5) – infrared: stars – stars: abundances – stars: fundamental parameters

1. Introduction

The properties of globular clusters and of their stellar populations provide fundamental information on the environment where galaxies formed, on the Galactic formation process, and are a basic ingredient for the understanding of the stellar populations in the external galaxies. Moreover, the properties of globular clusters are deeply connected with the history of their host galaxy. We believe today that galaxy collisions, galaxy cannibalism, as well as galaxy mergers leave their imprint on the globular cluster population of any given galaxy. Thus, when investigating globular clusters we hope to be able to use them as an acid test for our understanding of the formation and evolution of galaxies. The Galactic bulge is particularly important in the context of galaxy formation, as it is the only bulge that can be resolved into stars down to the bottom of the main sequence, and for which chemical abundances can be obtained with high-resolution spectra. Determinations of detailed chemical compositions are key data for studies of the origin and evolution of stellar populations, since they carry characteristic signatures of the objects that enrich the interstellar gas. The Galactic bulge globular clusters are relatively poorly understood stellar systems. The number of bulge globular cluster stars for which detailed chemical abundance information is available is considerably smaller compared to stars in halo clusters. Moreover, the advent of the new generation extensive surveys such as SDSS (Abazajian et al. 2009), 2MASS (Skrutskie et al. 2006), GLIMPSE (Benjamin et al. 2003), VISTA Variables in the Via Lactea (VVV) Public Survey (Minniti et al. 2010; Saito et al. 2012) yielded detection of several new Galactic Globular Clusters (GGCs). The December 2010 compilation of the Harris (1996) catalog included seven new GGCs not present in the February 2003 version, but several more cluster candidates have been proposed in the last years: SDSSJ1257+3419 (Sakamoto & Hasegawa 2006), FSR 584 (Bica et al. 2007), FSR 1767 (Bonatto et al. 2007), FSR 190 (Froebrich et al. 2008a), Pfleiderer 2 (Ortolani et al. 2009), VVV CL001 (Minniti et al. 2011), Mercer 5 (Longmore et al. 2011), VVV CL002 (Moni Bidin et al.

2011) and Kronberger 49 (Ortolani et al. 2012). Thus, detailed investigation of these newly discovered members of the globular cluster family can contribute significantly to the global understanding of the whole system. In this study we report the results of our high-resolution Phoenix spectroscopy of selected red giant stars of two newly-discovered globular clusters: 2MASS GC02 and Mercer 5, projected in the bulge area of the Galaxy. The globular cluster 2MASS GC02 was reported by Hurt et al. (2000) and was detected within the Two Micron All Sky Survey (2MASS). Later on Borissova et al. (2007) obtained deep infrared images and low-resolution K-band spectra. Based on the analysis of the J-Ks versus Ks color-magnitude diagram and spectroscopically derived metallicities and radial velocities of 15 stars they concluded that the cluster is moderately metal-rich ([Fe/H]=-1.1) and has a relatively high radial velocity. Its horizontal branch appears to be predominantly red, though the photometry can not rule out presence of a blue component as seen in NGC 6388 and NGC 6441. Comparison with the existing kinematic and abundance information for the GGCs indicates that 2MASS GC02 most probably belongs to the bulge sub-population, although inner halo association can not be ruled out. Recently, Alonso-García et al. (2014) discovered 29 new variables inside the tidal radius of 2MASS GC02, using the Vista varaibles in the Via Lactea (VVV) ESO Large Public Survey. Eight of these variables are classified as RR Lyr stars. Using these newly discovered RR Lyrae stars, they found that the extinction towards the cluster is highly differential, and seems to follow a non-standard law, thus putting the cluster closer to the galactic center (calculated distance of RGc = 2.2 Kpc).

The dust-obscured Galactic star cluster Mercer 5 was investigated by Longmore et al. (2011). The analysis of the near-infrared photometry from the United Kingdom Infrared Digital Sky Survey (UKIDSS) and the SofI/NTT near-IR spectroscopy, indicate that the object almost certainly is a Galactic Globular Cluster, located at the edge of the Galactic bulge. The cluster suffers strong and variable extinction, located at a distance of

approximately 5.5 kpc and is also moderately metal-rich ([Fe/H]=-1.0).

2. Data, Reduction and Analysis

Relevant information about our target clusters is presented in Table 1. Note that Mercer 5 is a newly discovered cluster (Mercer et al. 2005), still not included in the online version of the Harris (1996) catalog (2010 edition). Both globular clusters targeted for observations are located at low Galactic latitude, close to the plane of the Milky Way, in regions of high interstellar reddening (see Figure 1). Hence Phoenix high-resolution near-infrared echelle spectrograph (Hinkle et al. 1998) mounted at Gemini South 8-m telescope was a natural choice for the observations. The combination of large telescope aperture and high spectral resolution is crucial for accurate abundance determination, considering the apparent magnitudes of the individual red giants in our sample. More specifically, the data reported in Table 1 are taken from Longmore et al. (2011) (Mercer 5) and Borissova et al. (2007) (2MASS GC02). The fundamental parameters of both clusters are calculated using the technique outlined in Ferraro et al. (2006); Valenti et al. (2005) and Valenti et al. (2007), which allows to determine the reddening, distance modulus, and a global photometric metallicity of a globular cluster from its near-infrared CMD. In this case the RGB and HB clump calibrations were used. The targeted wavelength range was selected based on the line list published by Ryde et al. (2010) and covers a variety of Iron and α–elements metal lines. It also has the advantage of being devoid of bright OH airglow lines, which aids the analysis of faint spectral features. The Phoenix configuration that was used is presented in Table 2. Note that the spectral coverage provided by Phoenix is limited by the size of the science array and is much smaller than the bandwidth of the H6420 order-sorting filter.

Table 1: Information about the targeted clusters

ID	RA	DEC	l	b	D	$E(J-K)$	$(m-M)_0$	Ref.
	hh:mm:ss	dd:mm:ss	deg.	deg.	arcmin.	mag.	mag.	
(1)	(2)	(3)	(4)	(5)	(6)	(7)	(8)	(9)
2M GC02	18:09:37	-20:46:44	9.78	-0.62	1.9 ± 0.2	3.0 ± 0.1	13.54 ± 0.15	a, b
Mercer 5	18:23:19	-13:40:02	17.59	-0.11	0.60	2.1 ± 0.7	$14.29^{(1)}$	c, d

Notes: Column (1) is the cluster ID, followed by the equatorial coordinates of the object (columns (2) and (3)). The Galactic coordinates are presented in columns (4) and (5). Column (6) shows the apparent diameter of the cluster, followed by an estimate of the color excess E(J-K) in column (7). The distance modulus to the object is listed in column (8), followed by the list of the references to the various sources of information used in the table.

(1) The maximum $(m-M)_0$ value from Longmore et al. (2011) is considered.

References: (a) Borissova et al. (2007), (b) Hurt et al. (2000), (c) Mercer et al. (2005), (d) Longmore et al. (2011)

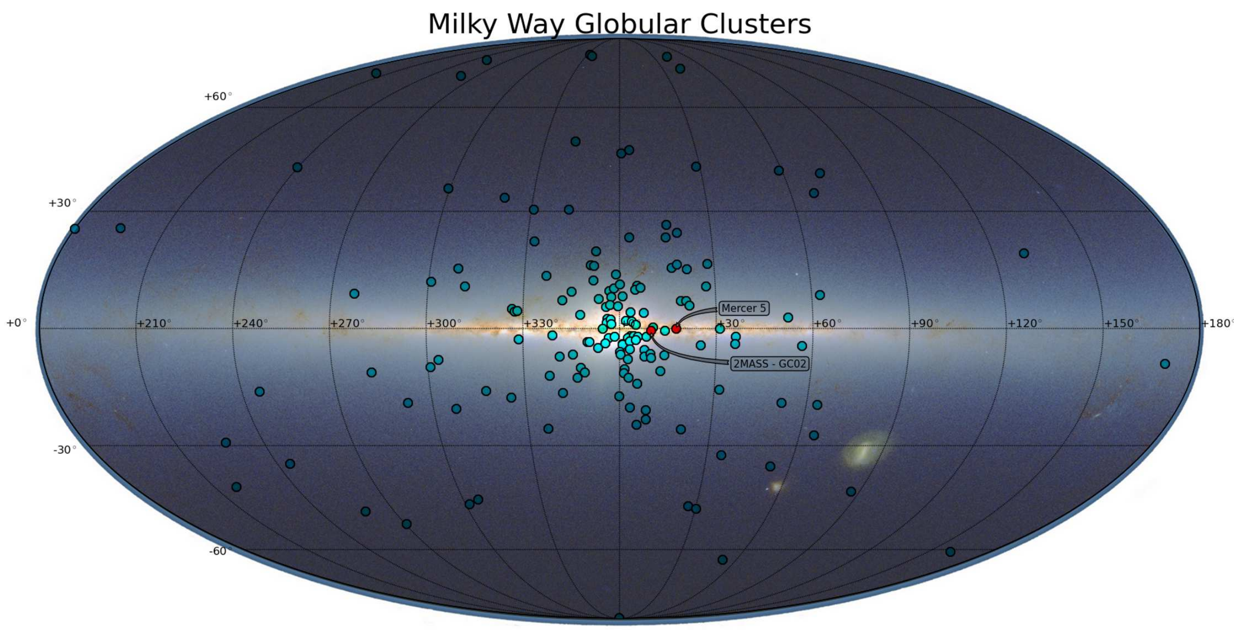

Fig. 1.— Illustration of the spatial distribution of the Milky Way Globular Clusters around the plane of the Galaxy. The two clusters targeted by the current study are marked and labeled. An elliptical projection of the Galactic coordinates was used with an all-sky image of the 2MASS stellar density set as a background.

2.1. Red Giant Stars Sample Selection and Observations

The stars observed in each cluster were selected on the basis of pre-existing Near-IR CMDs and low-resolution spectroscopy (SofI/NTT, R$\sim$1500 and ISAAC @ VLT, R$\sim$500). All of them were identified as high probability members of their host star clusters. The information about the individual stars observed is compiled in Table 3. We observed stars close to the Tip of the Red Giant Branch (TRGB) in order to ensure that the spectra will reach the required S/N ($\sim$ 60) with a sensible investment of observing time. Figure 2 shows the positions of the target stars in the clusters, and on their color-magnitude diagrams. The J, H and Ks images are taken from the Vista variables in the Via Lactea Survey (VVV, DR2, http://horus.roe.ac.uk/vsa/, Saito et al. (2012)) and UKIDS Galactic Plane Surveys (GPS,DR7, http://www.ukidss.org/index.html) and the three-color images are constructed. The CMDs of the clusters are build using the photometric catalogs provided in VVV and GPS and include all objects residing into a 60$''$ radius.

The spectra were acquired at Gemini South 8-m telescope during the semester 2010A (Program GS-2010A-Q-30, PI P.Pessev). Since our targets are relatively faint for such high spectral resolution (H$\sim$10-11), our observations took full advantage of the queue mode of operation, allowing us to impose exactly the required sky and seeing conditions during the data acquisition. A standard technique of ABBA offset pattern across the slit was used. Due to the crowded nature of the observed fields (see Figure 2) we did a quick pre-imaging for the Phoenix acquisitions and provided detailed finder charts for the queue observers. Telluric standards, of spectral class A or earlier, from the Gemini calibration library were observed either before or/and after the observations at matching airmass to ensure proper reduction and calibration. Since standard stars are significantly brighter than the science targets a larger offset along the slit (4$''$) was used, with respect to that of the science data (2.5$''$). According to the standard Gemini procedure, the exposure times for the tellurics

were adjusted by the night observer (depending on the luminosity of the particular star and the observing conditions at the moment of the observation) to provide sufficient S/N for high quality calibration. In general the exposure times for the standards were much shorter with respect to those of the science targets. Flat fields were taken each time science data were acquired, before moving the grating or changing the instrument configuration, using the dedicated 100W GCAL calibration source. Phoenix darks with exposure times matching the flat field data were secured at the end of each night. The calibration dataset was completed by wavelength calibration frames acquired with the internal Phoenix ThAr lamp. Considering the significant investment of observing time required and taking into account the narrow wavelength coverage of Phoenix (that does not provide a favorable configuration of calibration lines on the detector), these were taken only for a fraction of the data as an extra wavelength reference cross-check.

2.2. Data Reduction

The reduction of the spectra was carried out in the IRAF[1] environment, using the standard procedure for Phoenix data[2]. Here we provide only a brief outline, with a focus on some crucial steps. First we need to trim all the science and calibration frames. This is important because a small section of the detector array is delaminated and the first ∼ 50 rows of each image are infested with a lot of bad pixels. Skipping that step will cause unnecessary complications during the entire data reduction process. Further the flats and

---

[1]IRAF is distributed by the National Optical Astronomy Observatory, which is operated by the Association of Universities for Research in Astronomy (AURA) under cooperative agreement with the National Science Foundation.

[2]Available at: ftp://iraf.noao.edu/iraf/misc/phoenix.readme

Slit width		4	[pix.]
Slit width		0.34	[arcsec.]
Resolution ($\lambda/\Delta\lambda$)		$\sim$ 50000	
Central wavelength		$\sim$ 15537.5	[Å]
Wavelength coverage	min.	$\sim$ 15500.0	[Å]
	max.	$\sim$ 15575.0	[Å]
Width of the observed spectral region		75	[Å]
Filter used		H6420	

Table 2: Phoenix configuration used during the observations

Table 3: Observing log and information about the individual targeted stars

Cluster ID	StarID	RA	DEC	D cen.	H	Date Obs.	Exp. Time
		hh:mm:ss	dd:mm:ss	arcsec.	mag.	DDMMYYYY	sec.
(1)	(2)	(3)	(4)	(5)	(6)	(7)	(8)
2M GC02	Star 1	18:09:35.20	-20:47:02.20	32.56	10.7	04062010UT	7200
2M GC02	Star 4	18:09:36.50	-20:46:44.10	7.50	9.7	07062010UT	7200
Mercer 5	Star 1	18:23:19.08	-13:40:09.90	8.05	9.9	02072010UT	3000
Mercer 5	Star 2	18:23:19.58	-13:40:06.70	10.04	9.1	07062010UT	2400

Notes: Columns (1) and (2) are respectively the cluster and star ID, followed by the equatorial coordinates of the object (columns (3) and (4)). Column (5) is showing the distance between the individual star and the center of the corresponding cluster. The H magnitude of the object is given in column (6). The last two columns (7) and (8) are listing the UT date of the observation and the total exposure time used for the observations.

darks associated with each set of observations were combined and subtracted from the combined flats. The step of developing the normalized master flat for each set is particularly important, in order to properly remove the features due to variations in the slit illumination. Normalization is also crucial for the reduction of the telluric standards, to avoid spurious features affecting the final results. OH airglow lines were removed from both standard and science targets stellar spectra by subtracting each one of the ABBA pairs. Then the two-dimensional frames were divided by the normalized flat fields before the extraction of the individual spectra. The one-dimensional spectra were wavelength calibrated, using atmospheric OH airglow lines. We targeted a spectral region that contains multiple interesting lines of Iron and α–process elements being devoid of bright airglow features. This is particularly beneficial for the data reduction and the analysis of weak spectral lines, but poses significant challenges for the wavelength calibration. Most of the available atlases of the OH airglow are not suitable for analysis of such high-resolution data, especially taking into account the width of the analyzed spectral region (see Table 2). Fortunately the long exposures on the science targets allowed to identify five airglow features and assign the corresponding wavelengths using the The Arcturus Atlas (telluric lines) obtained with Phoenix at Kitt Peak[3] (Hinkle et al. 1995). The wavelength calibration solution was then cross-checked against the obtained arc lamp exposures. The telluric features in the final one-dimensional spectrum were corrected using the data for the corresponding standard stars. The resulting spectra for each of the stars in both 2MASS GC02 and Mercer 5 are presented on Figure 3.

---

[3]Available online at: ftp://cdsarc.u-strasbg.fr/cats/J/PASP/107/1042/

2.3. Analysis of the Obtained Spectra

Stellar spectra and chemical abundances were analyzed using the MOOG code (Sneden 1973). To perform the analysis the program relies on stellar atmospheres models and line lists of the atomic and molecular species in the studied wavelength range. The model atmospheres were computed with the ATLAS9 Kurucz, R.L. (1993) code. Recently a significant progress was achieved on the availability of the high resolution near-IR line lists, but it is still much more limited, compared to the optical wavelength range. Pioneering works of Wallace et al. (1996) and Hinkle et al. (1995) focused on hight-resolution, high signal-to-noise spectra of the Sun and Arcturus. Current effort is aimed on provide more uniform coverage across the HR diagram (see Lebzelter et al. (2012)). Although this is a massive improvement over the earlier situation, more data and further studies are needed to match the optical spectral atlases for reference stars. The line list we used was kindly provided by Nills Ryde (private communication). It covers 699 atomic and molecular lines in the 15500 - 15575 A wavelength region (see Table 6), including Iron lines, lines of α–elements and molecular lines (CN and OH).

MOOG computes synthetic spectra based input parameters, such as effective temperature, surface gravity, metallicity, micro-turbulence and α-elements abundance. In order to determine the effective temperature we used the photometry and low-resolution spectroscopy published by Borissova et al. (2002) and Borissova et al. (2007) for 2MASS GC02 and Longmore et al. (2011) for Mercer 5 in conjunction with the T_{eff}:color:[Fe/H] calibrations of Ramírez & Meléndez (2005) for giant stars. The initial effective temperatures used were 4000K for the 2MASS GC02 stars and 3600K for Mercer 5. Surface gravity ($log\ g$) has been estimated from theoretical evolutionary tracks using the location of the stars on the red giant branch Origlia et al. (1997). We performed spectral synthesis on suitable Fe I and Fe II lines to derive the metallicity. The micro-turbulence

velocity is set to a value typical for red giant stars (ξ_{micro}[km s^{-1}] = 2.13 - 0.23 log g) as given in Kirby et al. (2009). The adopted $[\alpha/Fe]$= 0.40 is set in accordance with Gonzalez et al. (2011). Their results are based on the analysis of 650 giants in the different sections of the Galactic Bulge. To fit the widths and shapes of the lines of the observed spectra, each synthetic spectrum was convolved with a gaussian function and macro-turbulence function and the abundance is allowed to vary until the best fit is identified. The selected spectral range gives a reasonable number of atomic and molecular lines not affected by blending to derive relative abundances (see Figure 3). Unfortunately it does not cover CO molecular lines. Therefore, we adopted three values of $[C/Fe]$ = -0.15, -0.35, and -0.55 in accordance with the results of Ryde et al. (2009) and Ryde et al. (2010). The total abundance errors were determined by varying each of the input stellar parameters by its estimated errors and adding in quadrature the resulting abundance variations (see Table 4). We estimate the typical uncertainties of $\Delta T_{eff}\pm$ 100K, Δ log g $\pm$ 0.2 dex, $\Delta\xi_{micro}\pm$ 0.5 km s^{-1}, which translates into abundance errors for Fe$\sim$0.14, N$\sim$0.10, O$\sim$0.11, Si$\sim$0.14, Ti$\sim$0.17, Ni$\sim$0.17, respectively.

3. Results

Figure 3 shows our best-fitting synthetic spectra superimposed on the observed spectra of the target giants in both globular clusters. The derived stellar parameters and element abundances are summarized in Table 4. By definition:

$$[X/Fe] = (log\epsilon(X) - log\epsilon(Fe)_{star}) - (log\epsilon(X) - log\epsilon(Fe)_{\odot}) \tag{1}$$

$$log\epsilon(X) = log\, n_X/n_H + 12, \tag{2}$$

where $log\, n_X$ is the number density of element X.

As mentioned before, the observed spectral interval does not cover the CO molecular

lines, hence we can not derive C abundance. To approach this we estimate the [N/Fe], [O/Fe], [Si/Fe], [Ti/Fe], [Ni/Fe] abundances for three distinct [C/Fe] values, consistent with the range reported for 14 red giants in the Galactic bulge by Ryde et al. (2009) and Ryde et al. (2010). As evident from the table, taking into account the uncertainties, most of the estimates for the individual giants are in agreement and only the [N/Fe] is affected by variations of [C/Fe]. In Table 5 we present the mean [O/Fe], [Si/Fe], [Ti/Fe], [Ni/Fe] abundances for each observed giant in Mercer 5 and 2MASS GC02 based on three estimates per star ([Fe/H] values for each star are also listed). For each cluster, [Fe/H] is calculated as the mean for the two giants, [O/Fe], [Si/Fe], [Ti/Fe], [Ni/Fe] are the mean of all the individual estimates. The uncertainties of the individual measurements were used to calculate the corresponding weights. The uncertainties reported in the table represent a conservative estimate, taking into account observational uncertainties, errors of calibrations, transformations and determination of the atmospheric parameters.

To compare our determinations with the abundance rations measured by previous authors we selected four bulge globular clusters: NGC 6522 (Barbuy et al. (2014)); NGC 6569 and NGC 6624 (Valenti et al. (2011)) and Terzan 1 (Valenti et al. (2014)); as well as the abundance measurements of 264 red giant stars in three bulge fields taken from Johnson et al. (2013). The results are shown in Figure 4 and Figure 5.

As can be seen from the plots, the two measured stars of Mercer 5 follow the general trend of both bulge field and cluster stars at this metallicity. Indeed, their [O/Fe], [Si/Fe] and [Ti/Fe] ratios are enhanced by $\geq + 0.3$. The 2MASS GC02 stars have relatively lower ratios, but still compatible with other bulge clusters. Therefore, abundance ratios alone would not allow us to confirm that these two objects are indeed bound globular clusters. On the other hand, the bulge metallicity distribution is populated only very sparsely at [Fe/H]$\sim$-1.0, therefore if those 4 were just bulge field stars, the probability of having all of

them so metal poor is virtually zero. Hence we confirm the cluster nature of both Mercer 5 and 2MASS GC02.

4. Summary

We present the first chemical abundance estimates of two newly discovered Galactic globular clusters, residing in the direction of the Bulge in regions of high interstellar reddening. [Fe/H] for 2MASS GC02 is in agreement with earlier estimate by Borissova et al. (2007) based on moderate-resolution near-IR spectroscopy in the K band. The metallicity for Mercer 5 is significantly higher than the value derived by Longmore et al. (2011) using SofI/NTT moderate-resolution spectra. Based on these results we conclude that both Mercer 5 and 2MASS GS02 are two intermediate metal reach Bulge globular clusters, with Iron abundances of [Fe/H]=-0.86 and [Fe/H]=-1.08, respectively. The [O/Fe], [Si/Fe] and [Ti/Fe] abundance rations of Mercer 5 are enhanced by $\geq +0.3$, with respect to solar value, while the two observed giants of 2MASS GC02 show lower rations.

Acknowledgements

Based on observations obtained at the Gemini Observatory, which is operated by the Association of Universities for Research in Astronomy, Inc., under a cooperative agreement with the NSF on behalf of the Gemini partnership: the National Science Foundation (United States), the National Research Council (Canada), CONICYT (Chile), the Australian Research Council (Australia), Ministério da Ciência, Tecnologia e Inovação (Brazil) and Ministerio de Ciencia, Tecnología e Innovación Productiva (Argentina). This paper is based on observations obtained with the Phoenix infrared spectrograph, developed and operated by the National Optical Astronomy Observatory. The data were acquired as part of science

program GS-2010A-Q-30 and 179.B-2002,VIRCAM, VISTA at ESO, Paranal Observatory. Support for JB,RK,SV,MZ is provided by the Ministry of Economy, Development, and Tourism's Millennium Science Initiative through grant IC12009, awarded to The Millennium Institute of Astrophysics (MAS) and Fondecyt Reg. No. 1120601 and No. 1110393. We acknowledge technical assistance by B. Idahl (CTIO REU 2013 program) on Figure 1. The authors are grateful to the anonymous referee for the constructive comments that improved the paper.

Facilities: Gemini:South(Phoenix)

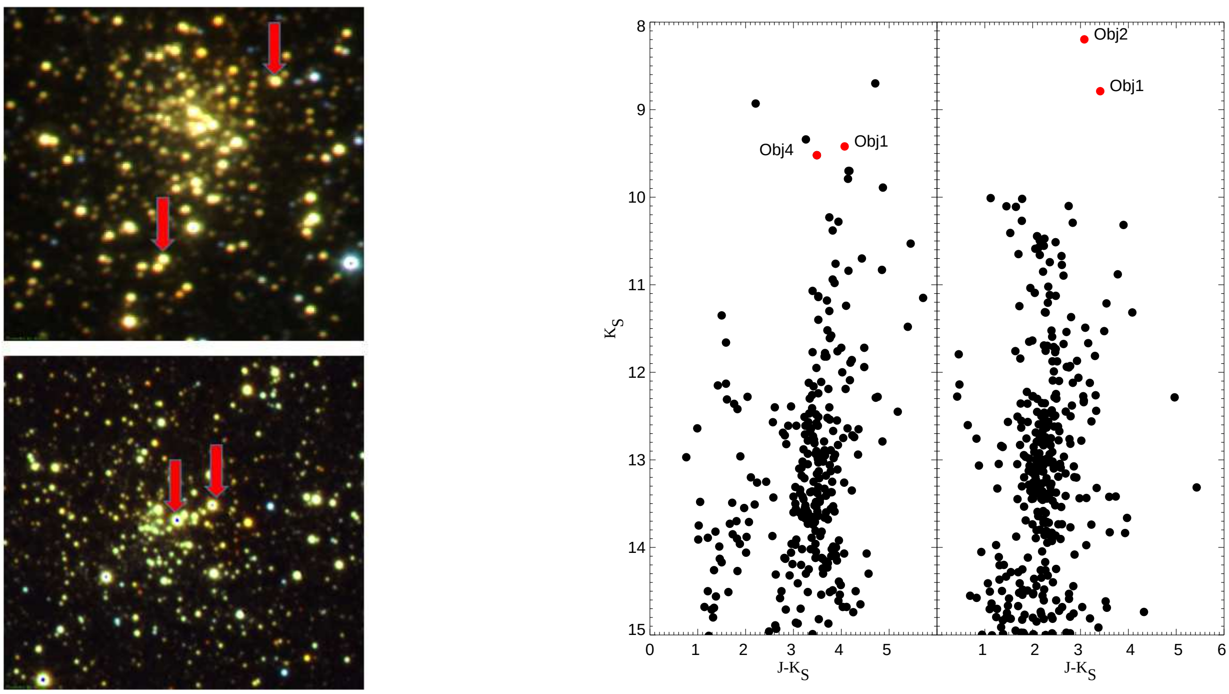

Fig. 2.— Illustration of the spatial distribution of the targeted red giants into the clusters and their positions on the CMDs. Left panel shows 1′ x 1′ three color images of the fields of GC02 and Mercer 5, taken from Vista variables in the Via Lactea (VVV) and UKIDS Galactic Plane Surveys. Right: The color-magnitude diagrams of the GC02 and Mercer 5 cluster fields. The black points represent all objects residing into a 60″radius; the observed objects are labeled.

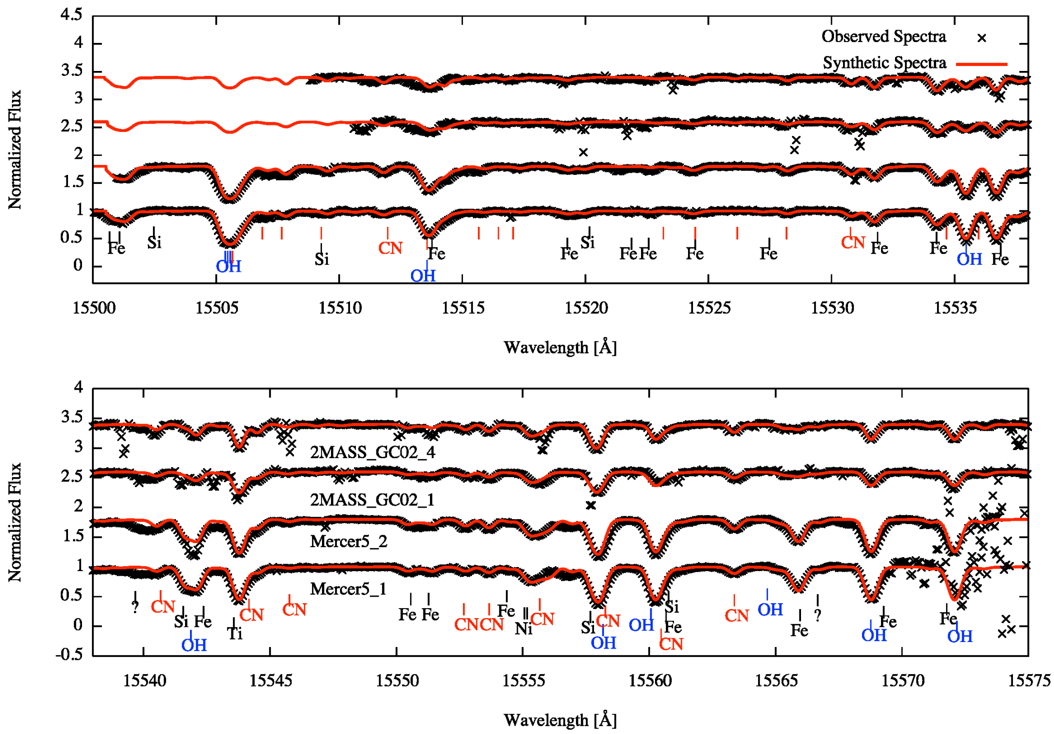

Fig. 3.— Observed spectra are shown with black crosses. Our best synthetic spectra are shown with a red line. Metal and Molecular lines are indicated below the spectra.

Table 4: Stellar parameters and derived abundances

	Mercer 5		2MASS GC02	
Object:	#1	#2	#1	#4
T_{eff} (K)	3650±100	3680±100	4000±100	4050±100
Log g ($cm\, s^{-2}$)	0.5±0.2	0.5±0.2	1.0±0.2	1.0±0.2
ξ_{micro} ($km\, s^{-2}$)	2.0±0.5	2.0±0.5	1.9±0.5	1.9±0.5
$[\alpha/Fe]$ (dex)	0.40	0.40	0.40	0.40
$[Fe/H]$ (dex)	-0.90±0.13	-0.80±0.14	-1.10±0.14	-1.05±0.14
		$[C/Fe]$ = -0.15 dex		
$[N/Fe]$ (dex)	+0.45±0.09	+0.65±0.10	+0.53±0.10	+0.43±0.10
$[O/Fe]$ (dex)	+0.30±0.11	+0.30±0.11	+0.12±0.12	+0.33±0.12
$[Si/Fe]$ (dex)	+0.50±0.14	+0.55±0.14	+0.03±0.15	0.00±0.15
$[Ti/Fe]$ (dex)	+0.30±0.17	+0.48±0.17	+0.20±0.17	+0.35±0.17
$[Ni/Fe]$ (dex)	+0.30±0.17	+0.25±0.17	+0.20±0.17	+0.10±0.17
		$[C/Fe]$ = -0.35 dex		
$[N/Fe]$ (dex)	+0.65±0.10	+0.95±0.10	+0.75±0.10	+0.70±0.10
$[O/Fe]$ (dex)	+0.30±0.10	+0.32±0.11	+0.10±0.12	+0.35±0.12
$[Si/Fe]$ (dex)	+0.50±0.14	+0.55±0.14	+0.05±0.15	+0.02±0.15
$[Ti/Fe]$ (dex)	+0.40±0.17	+0.48±0.17	+0.30±0.17	+0.35±0.17
$[Ni/Fe]$ (dex)	+0.30±0.17	+0.25±0.17	+0.15±0.17	+0.10±0.17
		$[C/Fe]$ = -0.55 dex		
$[N/Fe]$ (dex)	+0.90±0.10	+1.15±0.11	+1.03±0.10	+0.90±0.10
$[O/Fe]$ (dex)	+0.30±0.10	+0.32±0.11	+0.15±0.11	+0.30±0.11
$[Si/Fe]$ (dex)	+0.50±0.14	+0.55±0.14	+0.03±0.15	0.00±0.15
$[Ti/Fe]$ (dex)	+0.40±0.17	+0.48±0.17	+0.20±0.17	+0.40±0.17
$[Ni/Fe]$ (dex)	+0.30±0.17	+0.25±0.17	+0.15±0.17	+0.10 ±0.17

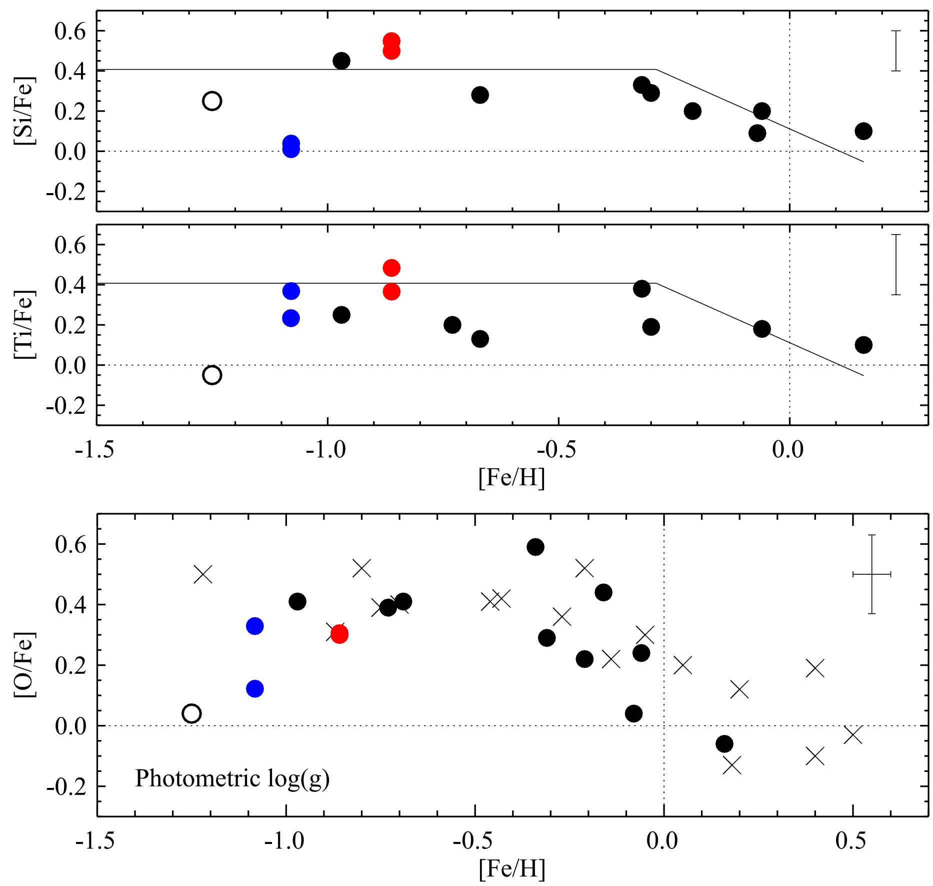

Fig. 4.— The ratios of O, Si and Ti to Iron (top to bottom). The dark circles stand for NGC 6522 red giant stars; blue, green and pink circles are for NGC 6569, NGC 6624 and Terzan 1 red giants, the Mercer 5 and 2MASS GC02 red giant abundance ratios from this paper are presented as red circles and are labeled.

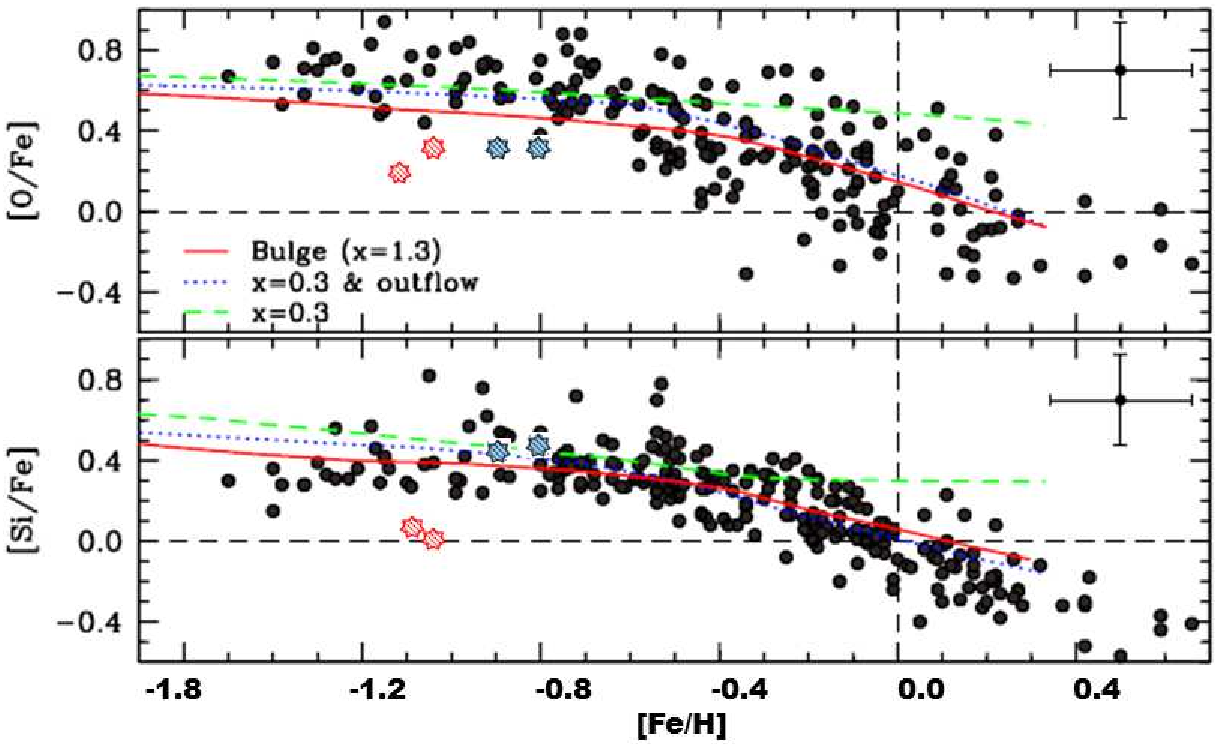

Fig. 5.— On the Fig. 18 of Johnson et al. (2013) are overplotted [O/Fe] and [Si/Fe] abundance rations of Mercer 5 (blue stars) and 2MASS GC02 (red stars) objects. The black circles are abundance rations of 264 red giants of three combined bulge fields; the solid red line shows the predicted change in each α-element as a function of [Fe/H], based on the bulge model of Kobayashi et al. (2011). The dashed green line is the model prediction assuming a flatter IMF (x=0.3) and the dotted blue line is the model prediction assuming x=0.3 with outflow (see Johnson et al. (2013) for details).

	Mercer 5			2MASS GC02		
	Object #1	Object #2	Mean	Object #1	Object #4	Mean
[Fe/H]	-0.90 ± 0.13	-0.80 ± 0.14	-0.86 ± 0.14	-1.10 ± 0.14	-1.05 ± 0.14	-1.08 ± 0.13
[O/Fe]	0.30 ± 0.11	0.31 ± 0.11	0.31 ± 0.11	0.15 ± 0.12	0.33 ± 0.12	0.23 ± 0.12
[Si/Fe]	0.50 ± 0.14	0.55 ± 0.14	0.53 ± 0.14	0.04 ± 0.15	0.00 ± 0.15	0.02 ± 0.15
[Ti/Fe]	0.37 ± 0.17	0.48 ± 0.17	0.42 ± 0.17	0.23 ± 0.17	0.37 ± 0.17	0.30 ± 0.17
[Ni/Fe]	0.30 ± 0.17	0.25 ± 0.17	0.28 ± 0.17	0.17 ± 0.17	0.10 ± 0.17	0.13 ± 0.17

Table 5: Derived abundances for both clusters. The mean [O/Fe], [Si/Fe], [Ti/Fe], [Ni/Fe] abundances for each observed giant in Mercer 5 and 2MASS GC02 are based on three estimates per star, ([Fe/H] values for each star are also listed). For each cluster, [Fe/H] is calculated as the mean for the two giants, [O/Fe], [Si/Fe], [Ti/Fe], [Ni/Fe] are the mean of the six individual estimates.

REFERENCES

Abazajian, K. N., Adelman-McCarthy, J. K., Agüeros, M. A., et al. 2009, ApJS, 182, 543

Alonso-García D´k´ny, I., Catelan, M., Contreras, R. Gran, F. at al. 2014, 2014arXiv1411.1696A

Barbuy, B., Chiappini, C., Cantelli, E., Depagne, E., Pignatari, M. et al. 2014 A&A, 570, 76

Benjamin, R. A., Churchwell, E., Babler, B. L., et al. 2003, PASP, 115, 953

Bica, E., Bonatto, C., Ortolani, S., & Barbuy, B. 2007, A&A, 472, 483

Bonatto, C., Bica, E., Ortolani, S., & Barbuy, B. 2007, MNRAS, 381, L45

Bonatto, C. & Bica, E. 2010, A&A, 516, 81

Borissova, J., Ivanov, V. D., & Vanzi, L. 2002, Extragalactic Star Clusters, 207, 107

Borissova, J., Ivanov, V. D., Stephens, A. W., et al. 2007, A&A, 474, 121

Ferraro, F., Valenti, E., and Origlia, L. 2006, AJ, 649, 243

Froebrich, D., Meusinger, H., & Davis, C. J. 2008, MNRAS, 383, L45

Gonzalez, O. A., Rejkuba, M., Zoccali, M., et al. 2011, A&A, 530, A54

Gonzalez, O. A., Rejkuba, M., Zoccali, M., et al. 2013, A&A, 552, A110

Harris, W. E. 1996, AJ, 112, 1487

Hinkle, K., Wallace, L., & Livingston, W. 1995, PASP, 107, 1042

Hinkle, K. H., Cuberly, R. W., Gaughan, N. A., et al. 1998, Proc. SPIE, 3354, 810

Hurt, R. L., Jarrett, T. H., Kirkpatrick, J. D., et al. 2000, AJ, 120, 1876

Johnson, C. I., Rich, R. M., Kobayashi, C., Kunder, A., & Koch, A. et al. 2013 ApJ, 765, 157

Kobayashi, C., Karakas, A. I., & Umeda, H. 2011, MNRAS, 414, 3231

Kirby, Evan N.; Guhathakurta, Puragra; Bolte, Michael; Sneden, Christopher; Geha, Marla C. 2009, ApJ, 705, 328

Kurucz, R.L. 1993, CD ROM, no 13

Lebzelter, T., Seifahrt, A., Uttenthaler, S., et al. 2012, A&A, 539, A109

Longmore, A. J., Kurtev, R., Lucas, P. W., et al. 2011, MNRAS, 416, 465

Marigo P., Girardi L., Bressan A., Groenewegen M. A. T., Silva L., Granato G. L.2008, A&A, 482, 883

Martini, P., Persson, S. E., Murphy, D. C., et al. 2004, Proc. SPIE, 5492, 1653

Mercer, E. P., Clemens, D. P., Meade, M. R., et al. 2005, ApJ, 635, 560

Minniti, D., Lucas, P. W., Emerson, J. P., et al. 2010, New A, 15, 433

Minniti, D., Hempel, M., Toledo, I., et al. 2011, A&A, 527, A81

Moni Bidin, C., Mauro, F., Geisler, D., et al. 2011, A&A, 535, A33

Nataf, D. M., Cassisi, S., & Athanassoula, E. 2014, MNRAS, 442, 2075

Origlia, L., Ferraro, F. R., Fusi Pecci, F., Oliva, E. 1997, A&A, 321, 859

Ortolani, S., Bonatto, C., Bica, E., & Barbuy, B. 2009, AJ, 138, 889

Ortolani, S., Bonatto, C., Bica, E., Barbuy, B., & Saito, R. K. 2012, AJ, 144, 147

Pietrinferni, A., Cassisi, S., Salaris, M., & Castelli, F. 2004, AJ, 612, 168

Ramírez, I. & Meléndez, J. 2005, ApJ, 626, 465

Roediger, J. C., Courteau, S., Graves, G., & Schiavon, R. P. 2014, ApJS, 210, 10

Rojas-Arriagada, A., Recio-Blanco, A., Hill, V., et al. 2014, arXiv:1408.4558

Ryde, N., Edvardsson, B., Gustafsson, B., et al. 2009, A&A, 496, 701

Ryde, N., Gustafsson, B., Edvardsson, B., et al. 2010, A&A, 509, A20

Saito, R. K., Hempel, M., Minniti, D., et al. 2012, A&A, 537, A107

Sakamoto, T., & Hasegawa, T. 2006, ApJ, 653, L29

Skrutskie, M. F., Cutri, R. M., Stiening, R., et al. 2006, AJ, 131, 1163

Sneden, C. 1973, ApJ, 184, 839

Valenti, E., Origlia, L. and Ferraro, F. R. 2005, MNRAS, 361, 272

Valenti, E., Ferraro, F. R., & Origlia, L. 2007, ApJ, 133, 1287

Valenti, E., Origlia, L., & Rich, R. M. 2011, MNRAS, 414, 2690

Valenti, E., Origlia, L., Mucciarelli, A., & Rich, R. M. 2014arXiv1412.2006V

Wallace, L., Livingston, W., Hinkle, K., & Bernath, P. 1996, ApJS, 106, 165

This manuscript was prepared with the AAS LaTeX macros v5.2.

,

Table 6. Line list used to model the observed spectra. The wavelength is in air, the excitation energy is of the lower level.

No.	Wav.[Å]	Elem.	$\chi_{\rm exc}$[eV]	No.	Wav. [Å]	Elem.	$\chi_{\rm exc}$[eV]	No.	Wav.[Å]	Elem.	$\chi_{\rm exc}$[eV]	No.	Wav.[Å]	Elem.	$\chi_{\rm exc}$[eV]
1	15500.073	ScI	4.50	176	15520.653	CN	3.76	351	15538.772	CN	3.75	526	15557.847	CN	2.65
2	15500.241	VII	9.04	177	15520.684	CN	3.36	352	15538.799	CN	4.15	527	15558.023	OH	0.30
3	15500.316	TiI	4.36	178	15520.855	CN	2.94	353	15538.854	CN	2.89	528	15558.045	CN	0.91
4	15500.345	CN	0.86	179	15520.893	OH	2.19	354	15538.903	CN	2.53	529	15558.176	CN	2.66
5	15500.650	MnI	6.20	180	15521.086	FeI	5.35	355	15539.060	CN	4.13	530	15558.585	TiI	4.50
6	15500.708	CN	2.58	181	15521.135	CN	4.00	356	15539.126	OH	0.79	531	15558.665	CN	0.73
7	15500.800	FeI	6.32	182	15521.207	CN	5.20	357	15539.330	CN	4.25	532	15558.880	CN	2.64
8	15501.003	CN	0.86	183	15521.245	CN	1.72	358	15539.417	CrI	5.96	533	15558.960	CN	2.87
9	15501.080	CN	3.15	184	15521.383	CN	2.40	359	15539.666	CN	2.53	534	15559.103	CN	2.42
10	15501.080	FeI	5.94	185	15521.515	CN	4.41	360	15539.673	CN	4.42	535	15559.500	NiI	5.87
11	15501.320	FeI	6.29	186	15521.690	FeI	6.32	361	15539.758	CN	3.29	536	15559.542	CN	1.01
12	15501.345	CN	3.29	187	15522.054	OH	2.83	362	15539.777	CN	5.82	537	15559.556	CN	2.67
13	15501.354	OH	3.10	188	15522.230	OH	3.12	363	15539.837	CN	0.88	538	15559.566	CN	1.00
14	15501.511	CN	0.99	189	15522.236	OH	2.73	364	15539.992	CN	5.16	539	15559.648	CN	1.01
15	15501.787	CN	2.84	190	15522.287	CN	2.94	365	15540.312	OH	3.48	540	15559.660	CN	1.00
16	15501.833	CN	2.58	191	15522.460	CN	4.21	366	15540.463	CN	3.98	541	15559.801	CN	1.00
17	15502.170	FeI	6.35	192	15522.600	CoI	6.21	367	15540.516	CN	0.88	542	15559.849	FeI	5.93
18	15502.239	CN	5.50	193	15522.640	FeI	6.32	368	15540.518	CN	3.77	543	15559.922	CaI	5.17
19	15502.261	CN	0.99	194	15522.672	OH	2.19	369	15540.898	CN	4.96	544	15559.973	CN	0.99
20	15502.294	OH	2.94	195	15523.041	CN	5.20	370	15541.125	CN	4.04	545	15560.135	CN	2.51
21	15502.429	CoI	3.41	196	15523.051	OH	2.73	371	15541.299	CN	3.98	546	15560.149	CN	1.01
22	15502.434	CN	3.98	197	15523.386	CN	3.72	372	15541.516	CN	5.73	547	15560.208	CN	1.00
23	15502.549	CN	2.84	198	15523.511	CN	1.45	373	15541.547	FeI	5.84	548	15560.244	OH	0.30
24	15502.564	CN	2.55	199	15523.591	OH	3.19	374	15541.557	CN	3.83	549	15560.270	CN	1.01
25	15502.576	CN	2.56	200	15523.807	CN	4.21	375	15541.644	OH	0.89	550	15560.287	CN	1.00
26	15502.640	SiI	7.13	201	15523.909	CN	0.88	376	15541.654	CN	4.42	551	15560.324	CN	3.71
27	15502.836	OH	3.44	202	15523.998	CoI	6.05	377	15541.818	CN	3.58	552	15560.578	CN	1.00
28	15502.934	CN	2.56	203	15524.003	CN	3.46	378	15541.850	CN	1.26	553	15560.685	CN	2.51
29	15503.043	OH	2.86	204	15524.277	NiI	2.74	379	15541.852	FeI	5.97	554	15560.704	CN	2.64
30	15503.246	ScI	4.17	205	15524.300	FeI	5.79	380	15541.857	FeI	6.37	555	15560.780	FeI	6.35
31	15503.246	CrI	3.38	206	15524.451	CN	0.88	381	15542.016	SiI	7.01	556	15561.041	CoI	6.08
32	15503.441	OH	2.72	207	15524.543	FeI	5.79	382	15542.090	SiI	7.01	557	15561.242	CN	3.72
33	15503.840	FeI	5.97	208	15524.615	CN	4.21	383	15542.090	FeI	5.64	558	15561.251	SiI	7.04
34	15503.943	CoI	5.73	209	15524.822	CN	2.55	384	15542.108	CN	0.83	559	15561.268	FeI	6.71
35	15503.967	VI	4.72	210	15524.832	CN	4.55	385	15542.146	OH	0.89	560	15561.399	CN	1.01
36	15503.994	CN	3.37	211	15524.847	OH	0.84	386	15542.173	CN	4.13	561	15561.457	CN	1.00
37	15504.083	CN	3.21	212	15525.227	FeI	5.84	387	15542.197	TiI	4.69	562	15561.523	CN	1.00
38	15504.126	CN	3.72	213	15525.360	CN	5.82	388	15542.205	CN	5.20	563	15561.535	CN	1.01
39	15504.554	CN	3.72	214	15525.406	CN	4.61	389	15542.297	CN	1.91	564	15561.748	CN	2.68
40	15505.107	CN	3.94	215	15525.435	CN	4.67	390	15542.316	CN	5.12	565	15562.080	VI	4.63
41	15505.326	OH	0.52	216	15525.495	CN	4.41	391	15542.611	CN	5.08	566	15562.131	CN	4.25
42	15505.350	CN	5.21	217	15525.514	CN	2.94	392	15542.731	TiI	4.39	567	15562.143	CN	2.50
43	15505.524	OH	1.43	218	15525.531	CN	2.72	393	15542.980	CN	1.20	568	15562.291	CN	1.15
44	15505.526	CN	1.45	219	15525.661	VI	4.88	394	15543.326	CN	4.00	569	15562.300	NiI	6.37
45	15505.591	CN	2.99	220	15525.734	TiII	8.10	395	15543.357	TiI	4.86	570	15562.436	CN	6.54

Table 6—Continued

No.	Wav.[Å]	Elem.	$\chi_{\rm exc}$[eV]	No.	Wav. [Å]	Elem.	$\chi_{\rm exc}$[eV]	No.	Wav.[Å]	Elem.	$\chi_{\rm exc}$[eV]	No.	Wav.[Å]	Elem.	$\chi_{\rm exc}$[eV]
46	15505.747	OH	0.52	221	15525.738	TiI	4.79	396	15543.633	CN	4.05	571	15562.441	CN	2.50
47	15505.771	TiI	4.39	222	15525.775	OH	3.51	397	15543.780	TiI	1.88	572	15562.460	CN	6.32
48	15505.782	OH	1.89	223	15525.775	CN	2.55	398	15543.785	OH	0.84	573	15562.601	OH	2.77
49	15505.846	CN	4.27	224	15525.934	CN	2.51	399	15543.838	TiI	4.79	574	15563.095	OH	2.77
50	15505.849	OH	1.43	225	15525.963	CN	4.21	400	15543.846	CN	3.58	575	15563.136	CN	3.58
51	15506.052	OH	2.85	226	15526.062	CN	2.84	401	15544.152	CuI	6.79	576	15563.139	OH	2.75
52	15506.079	CN	2.44	227	15526.083	CN	5.15	402	15544.355	TiI	2.49	577	15563.165	CN	4.29
53	15506.099	OH	1.43	228	15526.404	CN	1.00	403	15544.452	CN	2.72	578	15563.303	CN	1.00
54	15506.105	FeI	5.52	229	15526.414	CN	3.77	404	15544.501	CN	1.15	579	15563.306	CN	1.02
55	15506.246	OH	1.43	230	15526.604	CN	2.45	405	15544.680	CN	2.79	580	15563.315	CN	2.63
56	15506.246	OH	1.89	231	15526.819	CN	5.39	406	15544.730	CN	2.86	581	15563.354	CN	1.00
57	15506.252	ScI	4.97	232	15526.841	CN	3.84	407	15544.771	CN	4.00	582	15563.376	CN	1.15
58	15506.363	CN	4.26	233	15526.865	CN	4.55	408	15544.899	CN	4.47	583	15563.456	CN	1.02
59	15506.408	CN	4.91	234	15526.976	CN	2.72	409	15544.948	CN	2.51	584	15563.463	CrI	5.24
60	15506.685	CN	2.71	235	15527.043	CN	3.15	410	15545.047	CN	4.41	585	15563.778	CN	2.46
61	15506.779	CN	1.45	236	15527.210	FeI	6.32	411	15545.332	CN	2.72	586	15563.902	CN	2.79
62	15506.901	CN	6.39	237	15527.323	CN	3.90	412	15545.409	CN	5.63	587	15564.020	FeII	9.05
63	15506.969	CN	5.52	238	15527.325	CN	3.84	413	15545.511	CN	2.86	588	15564.185	CN	4.25
64	15506.980	SiI	6.73	239	15527.465	CN	2.57	414	15545.584	CN	1.15	589	15564.268	CN	2.75
65	15507.022	VI	4.87	240	15527.470	CN	2.94	415	15545.668	CN	5.82	590	15564.369	FeI	5.61
66	15507.043	PI	8.23	241	15527.513	CN	3.94	416	15545.782	CN	1.22	591	15564.684	CN	2.73
67	15507.046	CN	1.00	242	15527.535	SiI	7.14	417	15546.081	TiI	4.41	592	15564.723	ScI	4.53
68	15507.046	CN	3.21	243	15527.564	CN	4.61	418	15546.089	CN	2.60	593	15564.769	CN	2.69
69	15507.048	CN	2.99	244	15527.629	CN	4.55	419	15546.488	CN	2.60	594	15564.793	CN	2.75
70	15507.103	TiI	4.77	245	15527.713	OH	2.89	420	15546.531	CN	4.47	595	15564.938	OH	0.78
71	15507.118	FeII	8.94	246	15527.837	CN	2.57	421	15546.709	OH	3.48	596	15565.230	FeI	6.32
72	15507.156	CN	0.89	247	15527.890	CN	4.42	422	15546.780	CN	2.83	597	15565.256	CN	2.58
73	15507.180	CN	2.71	248	15528.109	FeI	5.95	423	15546.790	CN	4.47	598	15565.336	CN	2.42
74	15507.241	CN	0.71	249	15528.121	OH	1.35	424	15546.818	OH	2.75	599	15565.356	CN	0.91
75	15507.332	CN	5.21	250	15528.128	CN	4.92	425	15546.838	CN	1.22	600	15565.390	CN	4.05
76	15507.500	CN	4.49	251	15528.160	CN	2.96	426	15546.848	CN	5.44	601	15565.448	CN	1.76
77	15507.623	TiI	5.24	252	15528.218	CN	1.00	427	15546.920	CN	1.55	602	15565.588	CN	5.35
78	15507.816	CN	2.38	253	15528.365	CN	4.88	428	15547.041	CN	4.21	603	15565.644	CN	2.79
79	15507.844	CN	0.89	254	15528.575	CN	2.72	429	15547.940	OH	1.56	604	15565.734	CN	0.99
80	15508.075	CN	2.64	255	15528.577	CN	4.35	430	15548.190	CN	0.99	605	15565.770	CN	0.99
81	15508.385	TiI	4.77	256	15528.589	CN	2.67	431	15548.349	CN	3.67	606	15565.817	OH	0.90
82	15508.393	CN	4.80	257	15528.599	CN	4.67	432	15548.422	CN	4.47	607	15565.838	OH	3.66
83	15508.477	CN	1.22	258	15528.618	CN	3.77	433	15548.480	CN	3.89	608	15565.879	CN	1.02
84	15508.670	OH	1.89	259	15528.631	OH	3.06	434	15548.487	OH	3.66	609	15565.886	VI	4.64
85	15508.677	CN	6.07	260	15528.670	OH	3.21	435	15548.673	CN	2.87	610	15565.962	OH	2.78
86	15508.718	CN	2.64	261	15528.768	CN	3.94	436	15548.908	CN	2.61	611	15565.996	OH	0.90
87	15508.799	CN	0.97	262	15528.891	CN	4.41	437	15548.914	OH	0.93	612	15566.044	CN	1.02
88	15509.016	CN	3.46	263	15528.903	CN	2.94	438	15548.978	CaI	5.18	613	15566.051	CN	5.16
89	15509.507	CN	2.48	264	15528.915	CN	3.15	439	15549.206	CN	3.19	614	15566.255	CN	4.12
90	15509.526	CN	0.97	265	15528.994	CN	1.00	440	15549.501	CN	3.90	615	15566.274	CN	6.40

Table 6—Continued

No.	Wav.[Å]	Elem.	$\chi_{\rm exc}$[eV]	No.	Wav. [Å]	Elem.	$\chi_{\rm exc}$[eV]	No.	Wav.[Å]	Elem.	$\chi_{\rm exc}$[eV]	No.	Wav.[Å]	Elem.	$\chi_{\rm exc}$[eV]
91	15509.779	CN	2.48	266	15528.994	CN	3.06	441	15549.541	OH	2.59	616	15566.393	CN	4.96
92	15509.863	CN	2.70	267	15529.105	CN	4.92	442	15549.554	CN	2.83	617	15566.603	OH	2.68
93	15510.178	CN	4.20	268	15529.168	CN	2.96	443	15549.736	OH	2.18	618	15566.703	CN	2.63
94	15510.358	OH	1.89	269	15529.226	CN	5.84	444	15549.786	CN	3.90	619	15566.725	FeI	6.35
95	15510.648	OH	0.26	270	15529.243	CN	2.77	445	15549.803	CN	4.03	620	15566.907	CN	4.50
96	15510.717	CN	3.46	271	15529.316	OH	3.06	446	15549.902	OH	0.73	621	15566.941	CN	3.84
97	15510.847	CN	2.72	272	15529.344	CN	4.61	447	15549.948	CN	2.87	622	15567.001	ScI	4.97
98	15511.088	CN	4.20	273	15529.453	CN	2.72	448	15550.226	CN	4.10	623	15567.014	CN	3.94
99	15511.117	SiI	7.17	274	15529.657	OH	3.48	449	15550.320	CN	2.66	624	15567.188	SiI	7.11
100	15511.528	FeI	5.48	275	15529.662	CN	4.55	450	15550.357	CN	4.03	625	15567.261	FeI	6.35
101	15511.665	CN	5.73	276	15529.773	CN	3.15	451	15550.381	CN	0.89	626	15567.530	CN	6.42
102	15511.769	CN	5.52	277	15529.846	CN	4.67	452	15550.450	FeI	6.34	627	15567.552	OH	3.00
103	15511.810	CN	0.88	278	15529.913	CN	1.25	453	15550.553	CN	2.65	628	15567.575	OH	0.73
104	15512.147	CN	3.62	279	15529.928	CN	2.67	454	15550.560	FeI	6.11	629	15567.680	VI	4.62
105	15512.291	CN	2.37	280	15530.010	CN	2.64	455	15550.623	CN	3.19	630	15567.704	CN	5.16
106	15512.575	OH	0.86	281	15530.043	FeI	3.57	456	15550.645	CN	2.96	631	15567.724	CN	3.84
107	15512.635	CN	4.60	282	15530.080	CN	0.89	457	15550.867	CN	3.90	632	15567.728	VI	4.59
108	15512.724	VI	4.68	283	15530.162	CN	2.65	458	15550.949	CN	0.89	633	15567.869	CN	2.55
109	15512.761	CN	2.48	284	15530.186	CN	2.51	459	15550.964	CN	3.06	634	15568.180	CN	1.29
110	15512.771	OH	0.86	285	15530.195	VI	5.45	460	15550.981	CN	2.66	635	15568.187	SiI	7.11
111	15512.891	CN	0.82	286	15530.205	CN	3.06	461	15551.172	CN	5.44	636	15568.325	FeI	5.88
112	15513.146	CN	5.31	287	15530.316	CN	2.77	462	15551.430	FeI	6.35	637	15568.383	VI	4.67
113	15513.208	CN	1.12	288	15530.654	CN	2.64	463	15551.636	CN	2.89	638	15568.567	CN	4.96
114	15513.336	CN	2.67	289	15530.683	CN	4.30	464	15551.714	CN	4.14	639	15568.614	CN	2.69
115	15513.367	CN	3.54	290	15530.810	CN	0.89	465	15551.818	VI	4.66	640	15568.650	CN	2.45
116	15513.468	OH	0.92	291	15531.103	OH	3.29	466	15551.861	CN	2.65	641	15568.744	CN	0.99
117	15513.477	OH	0.26	292	15531.124	OH	2.94	467	15552.108	TiII	8.11	642	15568.764	CN	0.99
118	15513.511	TiI	4.51	293	15531.280	TiI	4.65	468	15552.222	FeI	5.62	643	15568.780	OH	0.30
119	15513.675	CN	1.06	294	15531.494	CN	4.84	469	15552.254	OH	2.74	644	15568.853	OH	3.29
120	15513.800	OH	0.92	295	15531.503	CN	4.61	470	15552.268	CN	3.89	645	15568.955	CN	2.86
121	15514.195	CN	2.53	296	15531.646	CN	3.15	471	15552.747	CN	0.90	646	15568.980	CN	4.50
122	15514.270	CN	1.12	297	15531.713	CN	3.12	472	15552.769	CN	3.89	647	15569.103	SiI	7.11
123	15514.280	FeI	6.29	298	15531.750	FeI	5.64	473	15552.885	CN	4.14	648	15569.135	CN	1.03
124	15514.427	OH	3.12	299	15532.116	CN	4.35	474	15553.245	VII	5.54	649	15569.240	FeI	5.51
125	15514.496	CN	1.06	300	15532.263	SiI	7.14	475	15553.313	CN	4.14	650	15569.314	CN	1.03
126	15514.691	SiI	7.09	301	15532.449	SiI	6.72	476	15553.340	CN	2.58	651	15569.486	CN	4.21
127	15514.802	CN	1.33	302	15532.536	CN	4.29	477	15553.560	FeI	5.48	652	15569.490	OH	0.84
128	15514.891	CN	1.52	303	15532.802	OH	3.48	478	15553.577	CN	2.89	653	15569.576	CN	4.74
129	15515.117	OH	2.21	304	15533.347	CN	4.29	479	15553.659	CN	1.08	654	15569.741	CoI	5.75
130	15515.368	TiI	2.31	305	15533.389	OH	1.35	480	15553.727	CN	2.58	655	15569.903	CN	2.61
131	15515.373	VI	4.65	306	15533.710	OH	2.33	481	15554.146	CN	4.41	656	15569.911	CN	2.40
132	15515.416	CN	2.38	307	15533.849	CN	0.99	482	15554.446	OH	0.79	657	15569.984	OH	2.78
133	15515.445	OH	2.18	308	15533.977	SiI	7.14	483	15554.501	CN	1.08	658	15570.044	CN	3.81
134	15515.617	OH	2.18	309	15534.020	CN	3.67	484	15554.510	FeI	6.28	659	15570.073	CN	3.70
135	15515.768	FeI	6.29	310	15534.081	CN	4.29	484	15554.510	fEi	6.28	660	15570.202	NiII	8.42

Table 6—Continued

No.	Wav.[$\AA$]	Elem.	$\chi_{\rm exc}$[eV]	No.	Wav. [$\AA$]	Elem.	$\chi_{\rm exc}$[eV]	No.	Wav.[$\AA$]	Elem.	$\chi_{\rm exc}$[eV]	No.	Wav.[$\AA$]	Elem.	$\chi_{\rm exc}$[eV]
136	15515.777	CN	2.50	311	15534.182	CN	3.36	486	15554.557	TiI	4.43	661	15570.306	CN	3.10
137	15515.797	CN	1.33	312	15534.260	FeI	5.64	487	15554.603	CN	1.28	662	15570.575	CN	3.41
138	15515.876	TiI	4.79	313	15534.306	OH	0.84	488	15554.625	VI	4.61	663	15570.752	CN	5.08
139	15515.931	CN	1.18	314	15534.368	CN	3.68	489	15554.697	VII	5.87	664	15570.861	CN	2.62
140	15515.969	OH	3.06	315	15534.399	CN	2.45	490	15554.855	CN	5.01	665	15571.055	CN	2.61
141	15516.151	CN	4.82	316	15534.455	CN	2.83	491	15554.939	OH	2.75	666	15571.099	VI	4.68
142	15516.284	OH	2.83	317	15534.602	CN	0.99	492	15555.112	OH	3.66	667	15571.120	FeI	5.88
143	15516.418	CN	1.00	318	15534.665	CN	4.13	493	15555.120	NiI	5.28	668	15571.152	CN	1.22
144	15516.537	OH	3.29	319	15534.892	CN	4.29	494	15555.138	CN	4.50	669	15571.220	CN	3.19
145	15516.660	OH	2.89	320	15534.986	CN	2.73	495	15555.210	NiI	5.28	670	15571.417	CN	4.21
146	15516.720	FeI	6.29	321	15535.167	CN	1.33	496	15555.370	NiI	5.49	671	15571.511	CN	5.35
147	15517.095	CN	2.77	322	15535.182	CN	4.27	497	15555.641	ScI	5.06	672	15571.664	CN	5.41
148	15517.228	OH	2.85	323	15535.317	CN	2.49	498	15555.700	CN	1.02	673	15571.729	VI	2.58
149	15517.275	CoI	5.74	324	15535.329	CN	3.91	499	15555.720	CN	1.36	674	15571.740	FeI	6.32
150	15517.367	CN	1.20	325	15535.353	CN	5.50	500	15555.750	CN	1.49	675	15571.822	CN	2.66
151	15517.487	CN	3.29	326	15535.462	OH	0.51	501	15555.765	OH	1.50	676	15571.834	CN	3.82
152	15517.815	CN	4.35	327	15535.498	CN	2.73	502	15555.835	CN	4.14	677	15571.897	CN	3.10
153	15518.135	CN	2.49	328	15535.602	CN	2.49	503	15556.016	NiI	5.28	678	15572.084	OH	0.30
154	15518.166	CN	2.77	329	15535.816	CN	1.06	504	15556.058	CN	4.04	679	15572.166	ScI	5.54
155	15518.289	CN	2.58	330	15535.829	CN	0.90	505	15556.106	OH	1.50	680	15572.217	CN	5.08
156	15518.395	CN	1.20	331	15536.224	CN	4.92	506	15556.115	OH	1.49	681	15572.230	OH	3.19
157	15518.670	CN	2.49	332	15536.642	CN	1.06	507	15556.122	CuI	6.55	682	15572.312	CN	0.84
158	15518.675	CN	2.58	333	15536.706	OH	0.51	508	15556.384	CN	4.30	683	15572.334	CN	0.99
159	15518.708	CN	4.14	334	15536.773	CN	2.71	509	15556.593	CN	1.02	684	15572.484	CN	2.66
160	15518.720	ScI	5.10	335	15536.895	OH	3.44	510	15556.670	FeI	5.93	685	15572.632	TiI	4.67
161	15518.764	CN	4.04	336	15536.997	CN	0.99	511	15556.711	TiI	5.30	686	15572.651	VI	4.65
162	15518.793	CN	1.23	337	15537.181	OH	0.84	512	15556.919	CN	4.04	687	15573.083	CN	1.03
163	15518.829	CN	5.07	338	15537.207	OH	0.78	513	15556.939	CN	1.36	688	15573.261	CN	1.49
164	15518.900	FeI	6.28	339	15537.227	CN	3.67	514	15556.962	OH	1.50	689	15573.277	CN	1.03
165	15519.065	CN	3.29	340	15537.253	CN	3.27	515	15557.006	CN	3.74	690	15573.294	CN	2.70
166	15519.084	CN	3.36	341	15537.410	OH	0.48	516	15557.006	CN	4.14	691	15573.466	CN	3.90
167	15519.100	FeI	6.29	342	15537.450	FeI	5.79	517	15557.212	OH	1.57	692	15573.673	CN	2.53
168	15519.360	FeI	6.29	343	15537.572	FeI	5.79	518	15557.387	CN	1.49	693	15573.724	CN	5.50
169	15519.600	CN	3.61	344	15537.690	FeI	6.32	519	15557.447	CN	3.74	694	15573.821	CN	4.68
170	15519.636	VI	4.11	345	15537.777	CN	4.13	520	15557.602	VI	4.68	695	15573.976	CrI	5.94
171	15519.942	FeI	2.48	346	15538.060	CoI	5.74	521	15557.607	CN	2.66	696	15574.060	FeI	6.31
172	15519.949	ScI	3.81	347	15538.081	CN	0.76	522	15557.684	CN	2.87	697	15574.599	CN	2.42
173	15520.115	SiI	7.11	348	15538.084	CN	5.20	523	15557.689	TiI	5.28	698	15574.667	CN	5.85
174	15520.154	CN	5.37	349	15538.434	OH	0.48	524	15557.735	CN	2.96	699	15574.837	CN	2.61
175	15520.262	CN	4.41	350	15538.463	SiI	6.76	525	15557.790	SiI	5.96				